

PACS numbers: 41.75.Jv; 52.38.Kd; 52.50.Jm; 42.65.Re; 32.80.Fb
DOI: 10.1070/QE2013v043n03ABEH015099

Production of multiply charged ion beams with an energy of tens of MeV/nucleon by ultrahigh-power laser radiation for nuclear physics problems

A.V. Korzhimanov, E.S. Efimenko, A.V. Kim, S.V. Golubev

Abstract. **We report a comprehensive analysis of an earlier proposed method which employs ultrahigh-power (petawatt) circularly polarised laser radiation to generate multiply charged ion beams in its interaction with a nanostructured two-component target; the ion beams are intended for application in nuclear physics. The problems of heavy atom ionisation in a superstrong laser field and laser-induced acceleration of the resultant ions to energies of ~20–30 MeV/nucleon are considered.**

Keywords: *laser acceleration, ion acceleration, multiply charged ions, petawatt lasers, nanostructured targets.*

1. Introduction

During the past decade, high-energy proton beam production with the use of superhigh-power laser pulses became the subject of active research – both theoretical and experimental (see, for instance, reviews [1, 2] and references therein). This is due to the large number of its possible applications, among which mention should be made of hadron beam therapy [3, 4], the fast ignition of targets in inertial confinement fusion [5], proton beam imaging [6], and ion source production for conventional accelerators [7]. Several schemes of laser-assisted ion acceleration were proposed, including acceleration by the surface layer of hot electrons, or target normal sheath acceleration (TNSA) [8, 9], acceleration by the shock wave at the target surface under irradiation [10], postacceleration in the relativistic transparency regime [the break-out afterburner (BOA) mechanism] [11], etc. For ultrahigh intensities (above 10^{20} W cm^{-2}), radiation pressure acceleration (RPA) [12–16] seems to be the most preferred method, for it is precisely this method that affords the highest acceleration efficiency. It is noteworthy that all of the methods listed above were studied only in the case of acceleration of protons and light ions (primarily carbon). At the same time, the problem of producing the beams of heavy ions with a high nuclear charge attracts considerable interest from the standpoint of nuclear physics, in the framework of the FAIR project [17] in particular.

Recently we pointed to the possible application of high-power lasers for generating and accelerating multiply charged ions with a medium nuclear charge [18]. The proposed scheme makes use of two-component structured targets of submicrometre thickness irradiated by a petawatt laser pulse. In this case, as shown in our work, efficient production of ion beams with a power and ion density unattainable with conventional accelerators is made possible under certain parameters.

In this work we undertake a more detailed analysis of the acceleration method proposed earlier, which may be represented as a two-stage process. At the first stage, a short high-contrast pulse with an intensity of 10^{20}–10^{22} W cm^{-2} interacts with the surface of a thin metal target and field-ionises the target atoms to provide a high degree of their ionisation (in particular, the estimated ion multiplicity is 24). At the second stage, the same laser pulse generates longitudinal electrostatic fields on the target surface, which are capable of accelerating the ions. To achieve a high efficiency in this scheme, a circularly polarised pulse should be normally incident on the target and the target itself should possess a lowered density, which may be practically achieved by using nanoporous targets. To obtain a monoenergetic beam, its acceleration is to be performed against the background of heavier ions, for instance gold, which may be realised with the use of gold targets with a thin layer of lighter atoms deposited on the surface under irradiation. The proposed scheme was tested by two-dimensional numerical particle-in-cell (PIC) simulations.

2. Ionisation in a laser field

In the investigation of the interaction of ultrahigh-intensity laser radiation with a substance containing multiply charged ions, one of the most significant and imperfectly understood problems is the charge-state distribution of the resultant ions. In this Section we consider the problem of estimating the ion multiplicity in a laser field with an intensity of ~10^{22} W cm^{-2}, but the elaborated methods also apply to a broader intensity range.

As already shown in earlier papers, the production of multiply charged ions under such intensities may proceed with a high efficiency [19, 20]. Here we put forward a simple model which permits estimating the degree of ionisation for arbitrary atoms with the requisite accuracy.

The ionisation of atoms by high-power radiation is usually considered in two limiting cases: multiphoton ionisation and dynamic tunneling ionisation. The adiabaticity parameter γ introduced by L.V. Keldysh [21] determines the character of photoionisation, with $\gamma^2 = I_p/(2\Phi)$, where I_p is the ionisation potential of an atom or ion; $\Phi = e^2E^2/(4m_e\omega^2)$ is the average electron oscillation energy in a strong laser field (or the ponderomotive potential); e and m_e are the electron charge and mass, respectively; ω is the frequency of laser radiation; and E is the electric field strength of laser radiation.

A.V. Korzhimanov, E.S. Efimenko, A.V. Kim, S.V. Golubev Institute of Applied Physics, Russian Academy of Sciences, ul. Ul'yanova, 46, 603950 Nizhnii Novgorod, Russia;
e-mail: korzhimanov.artem@gmail.com

Received 24 December 2012; revision received 12 February 2013
Kvantovaya Elektronika **43** (3) 217–225 (2013)
Translated by E.N.Ragozin

When $\gamma \gg 1$, the main ionisation mechanism is multiphoton ionisation, whose probability is $w = \sigma_n I^n$, where I is the radiation intensity; $n = 1 + I/(\hbar\omega)$ is the order of multiphoton ionisation; and σ_n is its cross section, which decreases strongly with increasing n. Multiphoton ionisation prevails for dielectrics with a low potential I_p; however, even for atomic gases with $I_p \sim 10$ eV and high-intensity laser USPs, tunnel ionisation mechanism [22] prevails even in the visible wavelength range; undoubtedly this is also true of lower lying levels with an ionisation potential of $10^2 - 10^3$ eV. The initial rigid condition $\gamma \ll 1$ for tunnel ionisation may be replaced with a milder condition $\gamma < 0.5$ [23]. To calculate the tunnel ionisation probability in a static field ($\gamma = 0$), wide use is made of the Perelomov–Popov–Terent'ev formula {formula (2.5) in Ref. [24]}, which is the generalisation of the formula for the ionisation probability for an arbitrary level of a hydrogen atom to different atomic or molecular system:

$$w_{\mathrm{PPT}}(|E|) = \omega_a \kappa^2 (2l+1) \frac{(l+m)!}{2^m m!(l-m)!}$$

$$\times C_{\kappa l}^2 2^{2n^* - m} F^{m+1-2n^*} \exp\left(-\frac{2}{3F}\right), \qquad (1)$$

where $\kappa = \sqrt{I/I_{\mathrm{H}}}$; I_{H} is the ionisation potential of hydrogen; $F = E/(\kappa^3 E_a)$ is the reduced electric field; $n^* = Z/\kappa$ is the effective principal quantum number; Z is the atomic nuclear charge; l and m are the angular momentum and its projection on the direction of electric field; $C_{\kappa l}$ is the dimensionless asymptotic coefficient of the wave function at a long distance r ($kr \gg 1$, where k is the wave number); $\omega_a = m_e e^2/\hbar^3 = 4.13 \times 10^{16}$ s^{-1} is the atomic frequency; and $E_a = m_e^2 e^5/\hbar^4 = 5.1 \times 10^9$ V cm^{-1} is the atomic field.

In experimental works, use is often made of another formula derived by Ammosov, Delone, and Krainov, which has come to be widely known as the ADK formula [25]:

$$w_{\mathrm{ADK}}(|E|) = \sqrt{\frac{n^{*3}}{Z^3}} \frac{FD^2}{8\pi Z} \exp\left(-\frac{2Z^3}{3n^{*3}F}\right), \; D = \left(\frac{4eZ^3}{n^{*4}F}\right)^{n^*}. \qquad (2)$$

It is pertinent to note that both formulas coincide asymptotically for large n^* and that formula (2) simplified for hydrogen-like atoms is of the form

$$w(|E|) = 4\omega_a \kappa^5 \frac{E_a}{|E|} \exp\left(-\frac{2\kappa^3 E_a}{|E|}\right), \qquad (3)$$

the ionisation probability for hydrogen atoms ($\kappa = 1$) coinciding with the well-known exact solution for the ionisation probability of the ground state of hydrogen atoms in a static electric field [26]. Equations (1)–(3) may be used for estimating the intensity required to ionise a level with a known ionisation potential, proceeding from the condition $w\tau \approx 1$ (τ is the pulse duration), although it should be admitted that this estimate is a simplified one and does not take into account in full measure the characteristics of the structure of an atom or ion. It is readily shown with the use of formula (3) that ions with nuclear charges $Z < 21$ are completely ionised in a laser field with an intensity of 10^{22} W cm^{-2} ($|E| \approx 2$ TV cm^{-1}) in 10 fs.

In what follows we shall use formula (1) for estimating the degree of ionisation for ions with a high nuclear charge. The results of numerical calculations for iron atoms are shown in Figs 1a and 1b. For simplicity of calculation, for the initial charge state distribution we adopted the single-ion species plasma of Fe^{21+}. One can easily see that there occurs a rapid (in a time shorter than one period of the laser field) ionisation

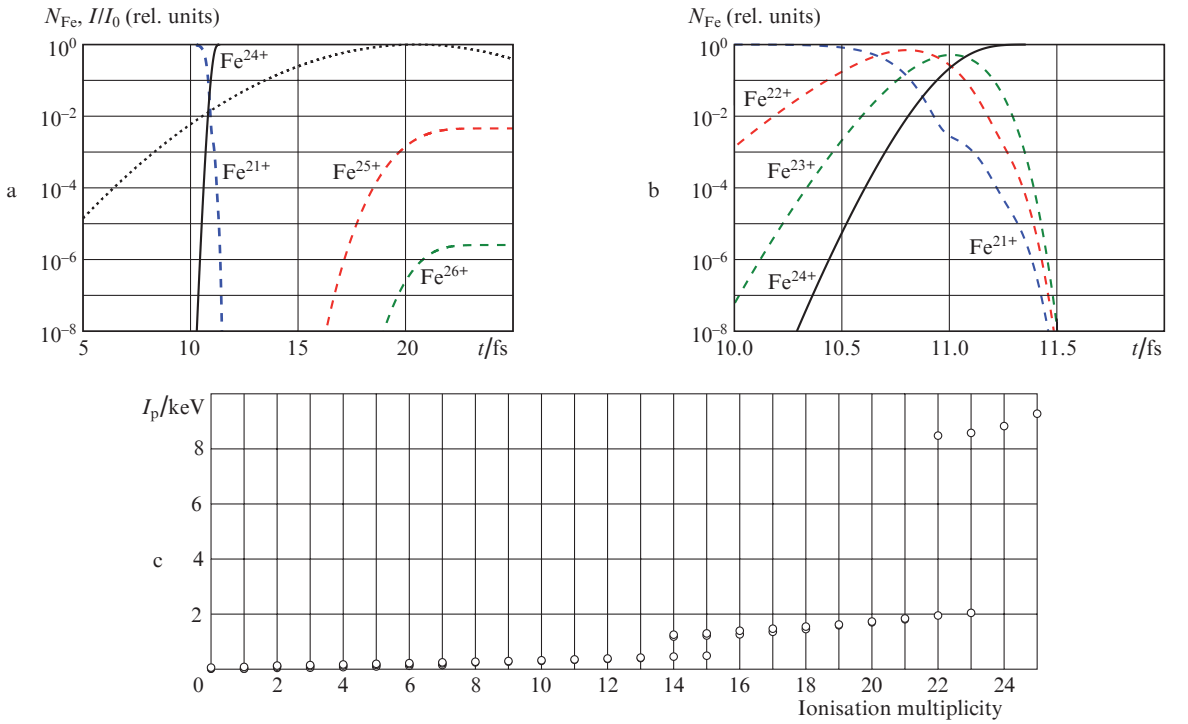

Figure 1. Dynamics of iron ion charge state distribution obtained from model (1) for a Gaussian laser pulse with a half-amplitude duration of 8 fs and a peak intensity of 10^{22} W cm^{-2} (the dotted line represents the pulse intensity profile normalised to the peak intensity I_0) (a, b), as well as dependence of the ionisation potential on the multiplicity of iron ions (different points for the same multiplicity correspond to electrons in different states) (c).

of virtually all ions to the Fe^{24+} state on the attainment of an intensity value of $\sim 10^{20}$ W cm^{-2}, with the result that a single charge state distribution is produced once again. This effect is robust in the sense that the ion charge state distribution is hardly changed if the intensity is further increased. An appreciable number (no less than 1%) of higher ionised particles appears only when the peak intensity is as high as 10^{22} W cm^{-2}. This circumstance justifies the use of the single charge state distribution, because including more subtle effects would slightly shift the ionisation threshold intensity, but would not change the result of ionisation qualitatively. Such a behaviour is characteristic for those multiply charged ions whose ionisation potential experiences significant steps in going from some orbital to a deeper one. By way of example, Fig. 1c shows the dependence of the ionisation potential of iron ions on their multiplicity: in going from 2s-shell electrons to 1s-shell electrons the ionisation potential increases by more than a factor of four.

Since the scheme of laser-driven ion acceleration proposed in our work relies on the use of targets consisting of two types of atoms, the heavier atoms serving as a background, we also estimated the multiplicities of the ions of gold atoms, which played the role of the background ones. With the use of model (1) it is possible to show that, as in the case of iron, all gold ions will have the same multiplicity (69+) with a high degree of accuracy.

Therefore, proceeding from the analysis outlined above, it is safe to say that the interaction of ultrahigh-power laser radiation with substance in a broad parameter range gives rise to ions with the same multiplicity, which may be estimated using a relatively coarse model (1). This conclusion, of course, must be thereafter verified by way of self-consistent numerical calculations with the inclusion of ionisation. However, the consideration of this problem goes beyond the scope of our paper.

We also note that, although the fields generated in the plasma may be of the same order of magnitude as the fields of laser pulses, their inclusion will not radically change the result obtained above, because the plasma fields effectively enhance the field acting on the ions by no more than a factor of one and a half–two, while their lifetime, as shown below, does not exceed the same few femtoseconds. At the same time, to radically change the ion charge state distribution will require an increase in the ionisation rate or the lifetime by at least one or two orders of magnitude.

3. Laser acceleration of multiply charged ions

The multiply charged ions produced in a laser field may be accelerated to a high energy by this field. Several methods of laser-driven ion acceleration are discussed in the literature; the TNSA and RPA methods are the most popular of them [2]. However, these methods have a serious drawback from the standpoint of accelerating multiply charged ions: at the point where the ions under acceleration are located the intensity of the electric field, which is responsible for efficient ionisation, is relatively low. Specifically, in the TNSA scheme the acceleration takes place from the rear target surface under the action of the charge separation field that results from the heating of electrons. The intensity of this field is usually considerably lower than the intensity of the laser field. As for the RPA scheme, the laser radiation–target interaction takes place only in the thin skin layer, in which the intensity of the laser field may be several orders of magnitude lower than at its maximum. Bearing this in mind, to accelerate multiply charged ions advantage should be taken of those methods in which the ions under acceleration are located directly in the field of the laser wave. We know (at least) two such schemes: acceleration by ponderomotively shifted electrons (APSE) [14] and acceleration in the BOA regime [11]. In the subsequent discussion we consider the feasibility of obtaining multiply charged ions by the APSE method.

The APSE method relies on the possibility of accelerating relatively light ions in the electrostatic field produced in the ponderomotive shifting of electrons on the surface of the layer of heavier ions. The shifting of electrons is more efficient in the case of circularly polarised radiation.

3.1. Analytical estimates

Let us determine how the ion acceleration energy depends on the two most important parameters of the system – the plasma density and the amplitude of a laser pulse. This problem is set forth at length and more rigorously in Ref. [14]; here we adduce a less rigorous, but a more lucid derivation.

When circularly polarised laser radiation with an amplitude E_0 is normally incident on a plasma layer with a sharp boundary, in the case of total reflection the ponderomotive pressure exerted on electrons is constant (not oscillating in time):

$$p_p = 2a_0^2, \tag{4}$$

where the pressure p_p is normalised to $m_e^2\omega^2c^4/(4\pi e^2)$; $a_0 = eE_0 \times (m_e c\omega)^{-1}$ is the normalised field amplitude; and c is the speed of light. On the other hand, when the ions are sufficiently heavy and the time intervals under consideration are short enough, this pressure is balanced by the electrostatic pressure arising from charge separation. If the electrons are shifted by a distance z_b into the plasma interior, the resultant electrostatic pressure can be estimated as

$$p_e = \frac{(n_0\zeta_b)^2}{2}, \tag{5}$$

where $\zeta_b = \omega z_b/c$ and $n_0 = 4\pi e^2 N_{e0}/(m_e\omega^2)$ is the plasma overdense parameter equal to the ratio between the unperturbed electron plasma density N_{e0} and the critical density for given laser radiation frequency. We equate the ponderomotive and electrostatic pressures to find the boundary of the shifted electron layer:

$$\zeta_b = \frac{2a_0}{n_0}. \tag{6}$$

Knowing the position of the shifted electron boundary it is possible to estimate the potential drop in the plasma layer. For this purpose we assume that the main contribution to the potential drop is made by the layer of bare ions (as shown in Ref. [14], this is true in a very broad parameter range). Then, the potential drop is

$$\Delta\varphi = \frac{n_0\zeta_b^2}{2} = \frac{2a_0^2}{n_0}. \tag{7}$$

Here, the potential $\Delta\varphi$ is normalised to the quantity $m_e c^2/e$. Therefore, the lower the plasma density for a constant radiation intensity, the higher the accelerated ion energy, which is proportional to the potential drop in the plasma layer. Hence there follows an evident conclusion: to maximise the ion beam

energy requires lowering the target density. This may be achieved, for instance, by employing nanoporous targets. It is pertinent to note that the use of a porous layer with a lowered plasma density was also proposed for increasing the accelerated ion energy by the TNSA technique [27, 28].

However, the density may not be lowered indefinitely. The matter is that the acceleration scheme under discussion is efficient only in a overdense plasma, i.e. there is an optimal plasma density, which permits obtaining ions with the highest energy. This density is defined by the threshold of relativistic self-induced transparency; and when a sharp boundary is irradiated by circularly polarised radiation, in the ultrarelativistic case the expression for this density is of the form [29]

$$n_0^{\text{th}} = \left(\frac{64a_0}{27}\right)^{1/2}. \tag{8}$$

It is easy to calculate that to the Ti:sapphire laser radiation (with a wavelength $\lambda = 800$ nm) with an intensity of 10^{22} W cm^{-2} there corresponds a dimensionless amplitude $a_0 \approx 50$. To this amplitude there corresponds an optimal overdense parameter $n_0 \approx 11$ or an unperturbed electron density $N_{e0} \approx 2 \times 10^{22}$ cm^{-3}.

On substituting expression (8) in formula (7) and multiplying the result of substitution by the charge of the ion under acceleration we obtain its energy in the optimal regime:

$$\varepsilon_{\max} \approx 1.3 Z_i a_0^{3/2} m_e c^2, \tag{9}$$

where Z_i is the ion charge. A simple estimate for $a_0 = 50$ and F_{56}^{24+} ions yields an energy of ~110 MeV per nucleon.

However, when considering a real situation, account must be taken of several factors responsible for a lowering of acceleration efficiency. Among them in the first place are the finite electron temperature {formulas (7) and (8) were derived under the assumption of cold electrons, the influence of thermal motion on the threshold of self-induced transparency was investigated in Ref. [30]} and the possible development of transverse instabilities in the interaction of laser radiation with the shifted electrons. Both of these factors elevate the self-induced transparency threshold (8) and thereby lower the ion energy. They are difficult to analytically take into account, and therefore we undertook numerical simulations to arrive at more realistic parameters for the generated ion beams.

3.2. One-dimensional numerical simulations

Numerical simulations of acceleration were performed in one- and two-dimensional geometries. The one-dimensional interaction problem was solved by way of numerical solution of the Vlasov–Maxwell system of equations. In doing this, the Vlasov equation was solved by the positive flux-conservative method (PFC) [31] and the Maxwell equations by the conventional FDTD method [32]. The numerical code was verified by comparing the resultant data with the analytical ones as well as with the data of independent particle-in-cell (PIC) simulations.

In the coordinate space the computational domain occupied 512 points, which corresponded to four incident radiation wavelengths. The target was a 800-nm thick layer ($0 < x < \lambda$) of gold ions Au^{69+}, which corresponded to one wavelength of Ti:sapphire laser radiation. We note that, for so high a multiplicity of gold ions, their charge-to-mass ratio is not much different from that for iron ions, and their dynamics may have an appreciable effect on the acceleration process. However, in order to expose more clearly the physical essence of the acceleration method under discussion, the gold ions were assumed to be immobile in our one-dimensional simulations. In the $0.05\lambda < x < 0.1\lambda$ interval inside the gold layer, all gold ions were replaced with a 40-nm thick layer of lighter F_{56}^{24+} ions. The electron density in the gold layer corresponded to the overdense parameter $n_{01} = 30$ ($N_{e01} \approx 5.1 \times 10^{22}$ cm^{-3}, $N_{Au} \approx 7.5 \times 10^{20}$ cm^{-3}) and in the iron layer to the overdense parameter $n_{02} = 60$ ($N_{e02} \approx 10^{23}$ cm^{-3}, $N_{Fe} \approx 4.3 \times 10^{21}$ cm^{-3}). The background plasma density was taken to be significantly higher than the optimal one [see formula (8)] in order to take into account the lowering of self-induced transparency threshold due to thermal effects.

In the momentum space the computational domain was different for different types of particles. For electrons it numbered 30000 points corresponding to the interval $(-150m_ec, 150m_ec)$ and for ions of both types it numbered 2000 points corresponding to the intervals $(-M_{Au}c, M_{Au}c)$ and $(-M_{Fe}c, M_{Fe}c)$ for gold and iron (M_{Au} and M_{Fe} are the masses of gold and iron atoms). The initial electron and ion temperatures were equal to 1 keV and 10 keV, respectively (the ion temperature was selected for considerations of convenience of numerical simulations: a lower temperature would have required too short a grid step in the momentum space and would not have exerted an appreciable effect on the interaction dynamics).

The incident laser pulse was Gaussian-shaped and had a peak intensity $I_0 = 10^{22}$ W cm^{-2}; the pulse duration was varied to achieve the optimal interaction regime. As noted in Ref. [14], there exists an optimal duration of the laser pulse, which maximises the accelerated ion energy. This is due to the following circumstances: on the one hand, too short a laser pulse may terminate earlier than the acceleration process and, on the other hand, too long a laser pulse shifts the electrons for too long a time and the accelerated ions overtake the electron layer under shifting, thereby falling out of the accelerating charge separation field.

Figure 2 shows the results of simulations with optimal parameters. The iron ion energy reached a maximum of 27 MeV nucleon^{-1} for a half-amplitude pulse duration $t_{FWHM} = 12\pi\omega^{-1} = 16$ fs. Special mention should be made of the fact that the ion beam is well localised both in space and in energy. The spread in energy does not exceed several percent. We also note that the ion energy spectrum extends up to a value of 36.5 MeV nucleon^{-1}, which agrees nicely with an estimate by formula (7).

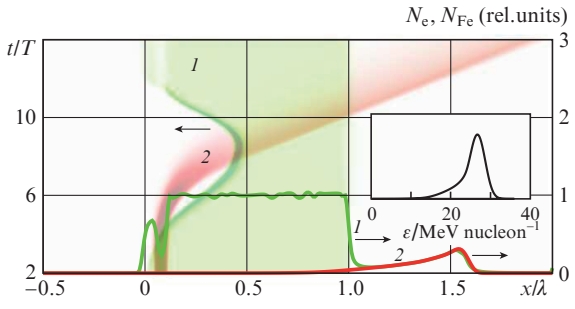

Figure 2. Spatio-temporal diagrams for electrons (*1*) and iron ions (*2*) as well as their spatial distributions at the points in time $t = 12T$ obtained in the one-dimensional numerical simulation of F_{56}^{24+} ion acceleration (T is the field period). Shown in the inset is the energy distribution function for iron ions at the same point in time.

3.3. Two-dimensional numerical simulations

We employed the ELMIS PIC code for two-dimensional simulations [33–35]. Its special feature consists in that it employs the fast Fourier transform for calculating electromagnetic fields. The computational domain in x, y coordinates measured 19.2×9.6 μm (i.e., $24\lambda \times 12\lambda$) and was an array of size 1024×512 cells. The gold layer thickness was equal to one wavelength (800 nm) and its width to eight wavelengths (6.4 μm). The longitudinal target structure and the particle densities were the same as in our one-dimensional simulation. The initial temperatures of all particles were equal to 16 keV. The plasma was irradiated by a laser pulse with a Gaussian envelope in the longitudinal direction. A fourth-order super-Gaussian envelope was selected for the transverse profile to lower the growth rate of transverse instabilities. The pulse width was equal to eight wavelengths and its duration was varied to find the optimal interaction regime.

Special mention should be made of the fact that the presence of transverse instabilities was one of the main factors which affected the results of our two-dimensional simulations. This gave rise, in particular, to some complications in the numerical simulations. A relatively high level on numerical noise is inherent in the PIC code, and this noise becomes the seed for rapidly growing instabilities. This has the effect that the data of numerical simulations turn out to be dependent on the parameter equal to the number of particles N_{ppc} in a spatial cell. Figure 3 shows the results of numerical simulations for the same parameters of the problem but for different N_{ppc}. As is clear from the drawing, for a small number of particles the emergent instability has a smaller scale and the highest energy of accelerated ions is lower than for a large number of particles. We discovered that the results cease to vary for $N_{ppc} > 2000$. All subsequent numerical simulations made use of precisely this value.

Figure 4 shows the results of two-dimensional simulations for three pulse durations. In Figs 4b and 4e the duration is optimal, $t_{FWHM} = 6\pi\omega^{-1} = 8$ fs. It is noteworthy that, in contrast with the one-dimensional simulations, the selection of optimal pulse duration was affected primarily by the transverse instability, which disturbed the process of acceleration for sufficiently long pulses. Figures 4a and 4d show the results of simulations for a shorter pulse duration. In this case, the pulse terminates prior to the completion of acceleration, with the consequence that the resultant ion beam is widely dispersed both in space and in energy: a part of the ions have managed to accelerate and a part of them have not. For a pulse duration longer than the optimal one (Figs 4c and 4f) the development of transverse instabilities becomes quite evident, which affects the spatial beam quality as well as the beam acceleration efficiency.

In the optimal regime, iron ions exhibit a strongly pronounced energy peak about 28.2 ± 0.4 MeV nucleon^{-1}. Interestingly, in the two-dimensional case the scatter in ion energy turned out to be substantially narrower than in the one-dimensional case. This fact is explained as follows: the initial stage of acceleration by the method of ponderomotively shifted electrons is followed by the stage of directional Coulomb expansion of the two-component target. It was missing from the one-dimensional simulations because gold ions were assumed to be immobile. Two ion fractions are separated at this stage: the lighter ions turn out to be ahead of the heavier ions (Fig. 5a) and acquire the same speed equal to the highest energy of the heavier ones (Fig. 5b). This process is demonstrated by Fig. 5c, which shows the time dependence of accelerated ion energy distribution. It is also noteworthy in this case that the iron ions gain a substantial fraction of their energy during precisely the second stage – the Coulomb expansion. A similar effect in the case of ion acceleration by radiation pressure was described in Ref. [36]. In this case, the

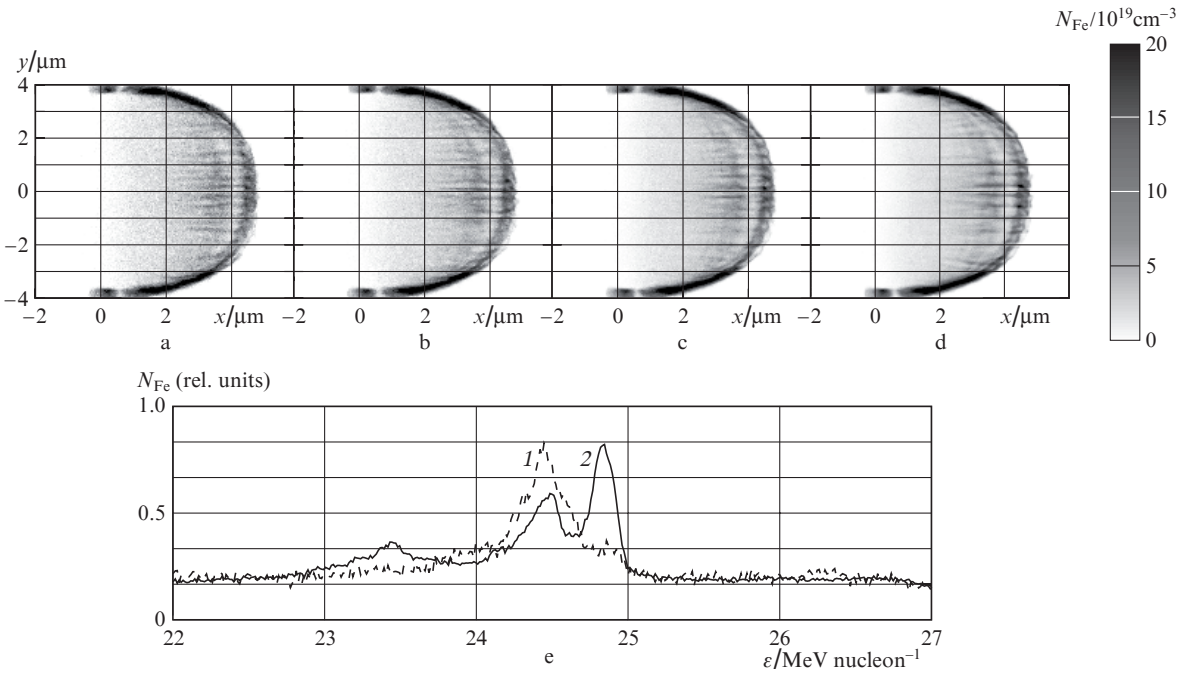

Figure 3. Results of two-dimensional numerical simulations of iron ion acceleration for a different number of particles in a cell for a pulse duration of 10.7 fs and the remaining parameters specified in the text: spatial distributions of accelerated ion density for $N_{ppc} = 250$ (a), 500 (b), 1000 (c), and 2000 (d), as well as accelerated ion energy distributions for $N_{ppc} = 250$ (*1*) and 2000 (*2*) (e).

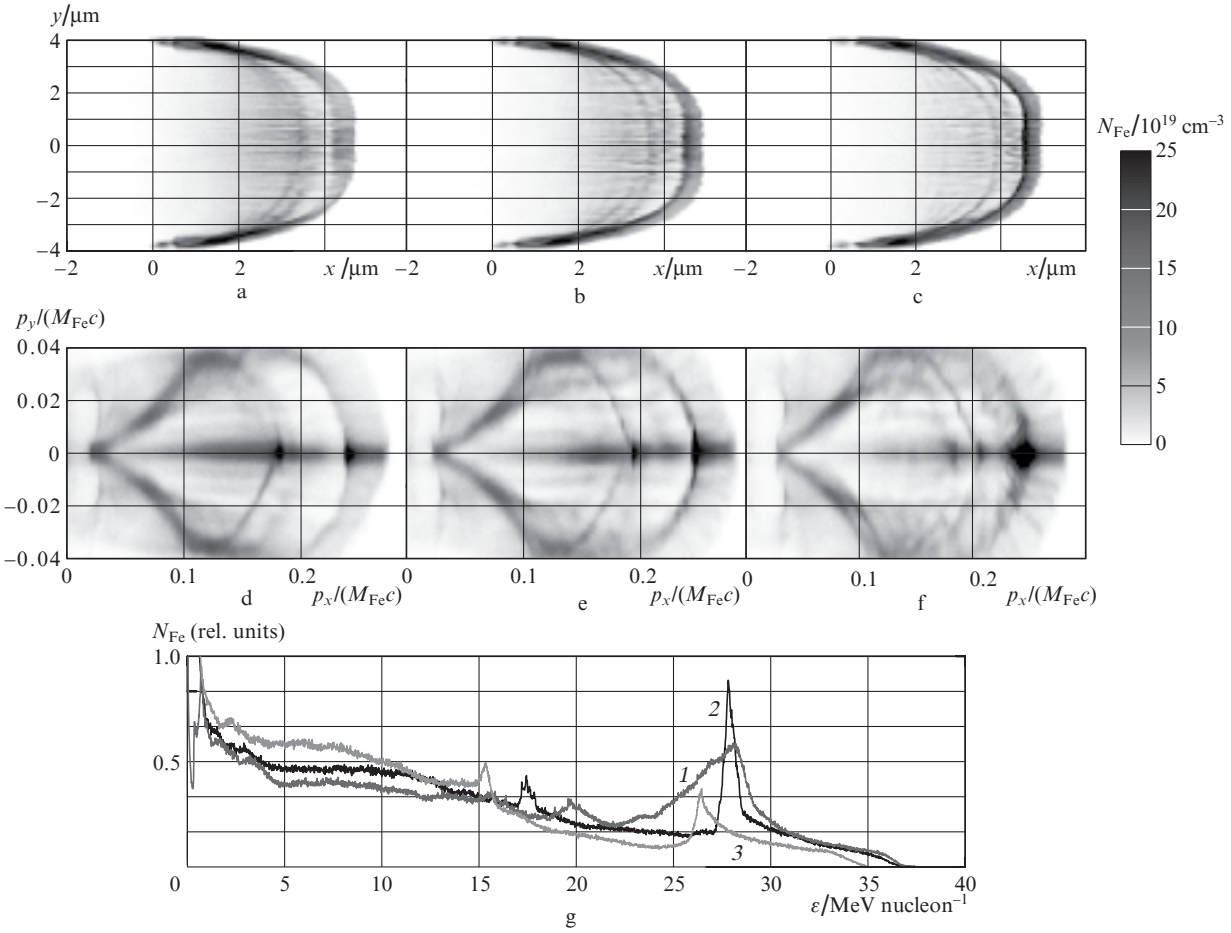

Figure 4. Results of two-dimensional numerical simulations of iron ion acceleration for different durations of laser pulses (the simulation parameters are specified in the text): the spatial distributions of accelerated ion densities (a–c) and the phase planes of accelerated ions (d–f) for a pulse duration of 6.7 (a, d), 8 (b, e), and 9.3 fs (c, f), as well as accelerated ion energy distributions for a pulse duration of 9.3 (1), 8 (2), and 6.7 fs (3) (g).

very idea of employing multicomponent targets for obtaining monoenergetic accelerated-ion distributions had also been discussed earlier (see, for instance, Section 3.6 in Ref. [1] and references therein), and the energy peak narrowing in the expansion of a two-component plasma was pointed out, for instance, in Ref. [37], where this effect was termed Coulomb piston. The theory of this effect was further elaborated also in Ref. [38].

A special feature of the two-dimensional simulation which distinguishes it from the one-dimensional one is that the plasma beam resulting from acceleration is not quasi-neutral. This is obviously due to the fact that Coulomb forces decrease with distance in a multi-dimensional case. The presence of an overall charge of the resultant beam may be used for its subsequent acceleration by conventional accelerators. At the same time, the presence of an overall charge can be a negative factor responsible for the Coulomb explosion of the resultant beam and for impairment of its characteristics.

It should be noted that, according to formula (7), in the model under discussion the energy acquired by the lighter ions depends only on the target density, but is independent of the target thickness. This distinguishes the present acceleration method from other schemes: in particular, lowering the target thickness to some optimal value for a constant target density increases the energy of ions accelerated by radiation pressure [36], while the energy itself is determined by the target column density rather than the volume one (see, for instance, Ref. [39]). This is due to the following fact: in contrast with radiation pressure acceleration method, in the acceleration by ponderomotively shifted electrons the heavier ions play the role of a background and no other, and the acceleration takes place in a thin target surface layer. To verify the proposition that the energy acquired by iron ions is independent of the target thickness, we performed simulations whose results are demonstrated in Fig. 6. One can see that lowering the target thickness has no or little effect on the energy of accelerated ions. Some increase in energy with a decrease in thickness is due to its effect on the energy of gold ions, which determines the additional energy acquired by iron ions in the course of Coulomb expansion. At the same time we emphasise that the monoenergetic peak formation and, therefore, efficient iron ion acceleration do not take place when the target thickness is smaller than some threshold. This is due to the relativistically induced transparency of the thin foil, in which the electron column density becomes lower than the critical value defined by the expression (see, for instance, Ref. [15])

$$\sigma_{cr} = n_0 L_{cr} = 2a_0, \tag{10}$$

where the critical target thickness L_{cr} is normalised to c/ω.

We also emphasise that the ion acceleration scheme proposed in our work necessitates the use of circularly polarised radiation. Despite the fact that the employment of linearly

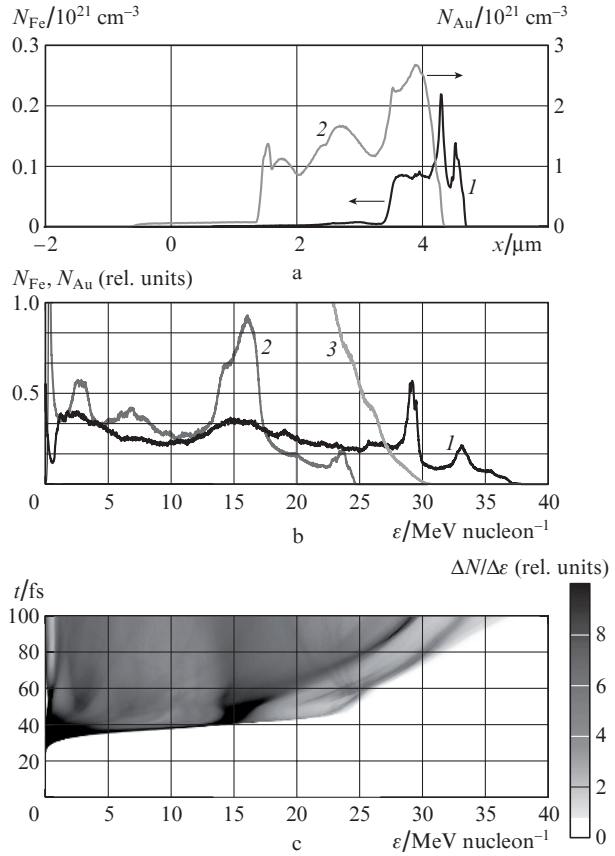

Figure 5. Results of two-dimensional numerical simulations of iron ion acceleration for a pulse duration of 13.3 fs: iron (*1*) and gold (*2*) ion density distributions along the x-axis at the point in time 100 fs after the beginning of simulation (a), energy distributions for iron ions at the points in time 100 (*1*) and 50 fs (*2*) and for gold ions at the point in time 100 fs (*3*) (b), as well as the dependence of iron ion energy distribution on the time elapsed since the beginning of simulation (c); ΔN is the number of ions with energies between ε and $\varepsilon + \Delta\varepsilon$.

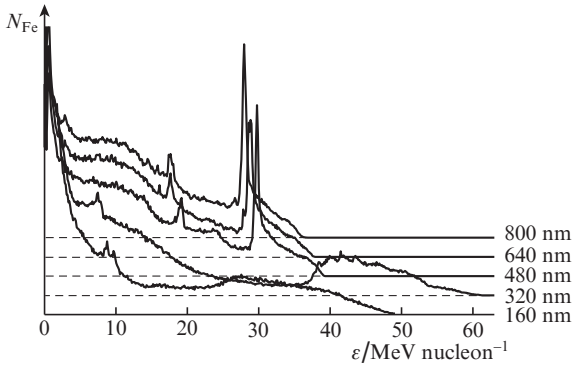

Figure 6. Energy spectra of iron ions obtained by two-dimensional numerical simulations of their acceleration by an 8-fs long laser pulse for a target thickness ranging from 160 to 800 nm (which corresponds to 0.2λ and λ). For visual clarity the abscissas for different thicknesses are shifted along the ordinate axis.

polarised radiation of the same power leads, as a rule, to an increase in generated ion energy (usually because of impairment of the beam quality) [16, 40], in the acceleration scheme under discussion a significant part is played by the formation of a stable charge separation field at the irradiated target surface due to efficient electron shifting. This shifting does not take place when use is made of linearly polarised radiation, because the electrons execute longitudinal oscillations with a period equal to one half of the period of the laser field. Consequently, efficient acceleration does not take place at the initial interaction stage, which has to provide the greater part of the momentum acquired by the electrons. This statement can be illustrated by comparing Fig. 7 and Fig. 5c, which show the energy spectra of the ions accelerated respectively by linearly and circularly polarised pulses of equal power and equal duration. Observed in the latter case is high-efficiency acceleration during the time interval $t = 35-45$ fs, with the result that the bulk of ions acquire an energy of $\sim$15 MeV nucleon^{-1} (which is slightly more than one half of their final energy), while in the former case this process does not occur and the final energy of even the highest-energy ions is lower. This feature is even more pronounced for shorter pulses, which form the highest-quality beams.

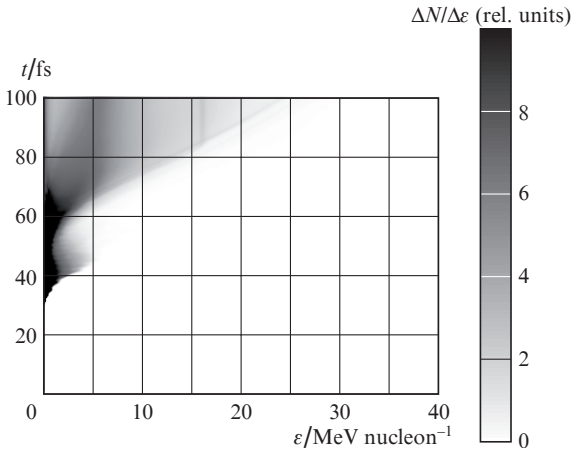

Figure 7. Dependence of iron ion energy distribution on the time elapsed since the beginning of simulation, which was obtained in the two-dimensional simulation of iron ion acceleration by a linearly polarised 13.3-fs long pulse with a peak intensity of 2×10^{22} W cm^{-2}.

Two-dimensional simulations permit estimating the total charge and current of the beam as well as the degree of its collimation. According to our simulations, the total number of accelerated ions (if the beam size in the direction of the z axis is assumed to be equal to its size in the direction of the y axis) amounts to 1.8×10^9 particles and their charge to 7 nC. The resultant beam is 5 fs long, which corresponds to a current of 1.4 MA. The total energy imparted to the beam is equal to 0.5 J, i.e. to $\sim$0.2% of the initial energy of the laser pulse. The beam emittance is equal to $5 \times 10^{-3}\pi$ mm mrad and the peak power of the beam to 80 TW, which is two orders of magnitude higher than the figure projected in the framework of the FAIR project [17].

However, it is noteworthy that the pulse duration in the optimal regime amounts to only 8 fs, which is, by all appearance, unattainable for modern petawatt laser systems in the near future. An increase in pulse duration impairs the quality of the generated ion beam, although its ion energy may be higher than in the optimal regime by virtue of the fact that the energy of the longer pulse is higher and may be transferred the ions under acceleration in the course of directional Coulomb explosion. Relatively good results are obtained, in particular,

for 15-fs long pulses (Fig. 8). These pulses may theoretically be obtained with the use of Ti:sapphire systems. However, for more realistic durations (~30–40 fs) the acceleration process is almost totally disrupted by the development of transverse instabilities (they, as a matter of fact, may be compensated by increasing the plasma density, which, however, has an adverse effect on the accelerated ion energy).

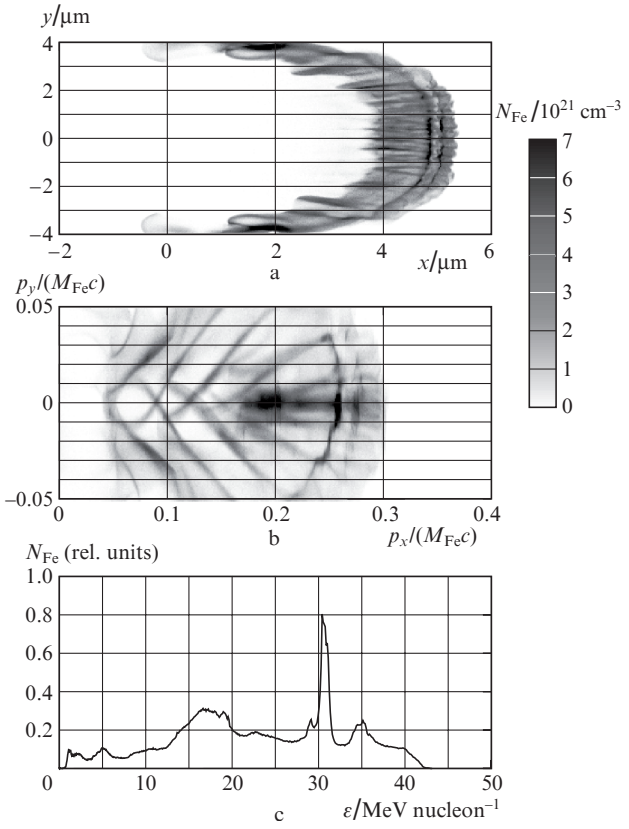

Figure 8. Results of two-dimensional simulations of iron ion acceleration by a 15-fs long laser pulse (see body of text for the simulation parameters): spatial distribution of iron ion density (a), phase plane of iron ions (b), iron ion energy distribution (c).

At the same time it should be noted that the total pulse duration is not as important for acceleration as is the rate of its rise. Recent discussion has been focused on the employment of the so-called relativistic shutter for controlling the leading edge of an ultrahigh-power pulse [41]. The idea of such a shutter consists in the use of a superthin (of the order of several nanometres) metal foil, which completely reflects laser radiation under normal irradiation. However, when the radiation intensity exceeds some threshold value, the velocity of motion of all electrons in the foil approaches the speed of light, resulting in a drastic decrease in its reflectivity [42, 15]. In this case, the transmitted pulse may have a very sharp leading edge – as short as one half-cycle of the field.

The idea of a relativistic shutter may be used for profiling laser pulses suitable for use in the proposed acceleration scheme. We investigated this possibility by way of numerical simulation. In contrast with the ordinary scheme, a 270-nm thick gold layer with a density of 7.5×10^{20} cm^{-3} was placed in front of the main target at a distance of 1 μm (the density was selected from considerations of simplicity of numerical simulation and the thickness was selected in such a way that the foil bleaching occurred near the intensity peak of the incident pulse). The pulse duration was equal to 30 fs. The results of simulations are shown in Fig. 9. The resultant ion beam has a poor quality, but a high energy. It is likely that some optimisation of this scheme will permit obtaining higher-quality beams.

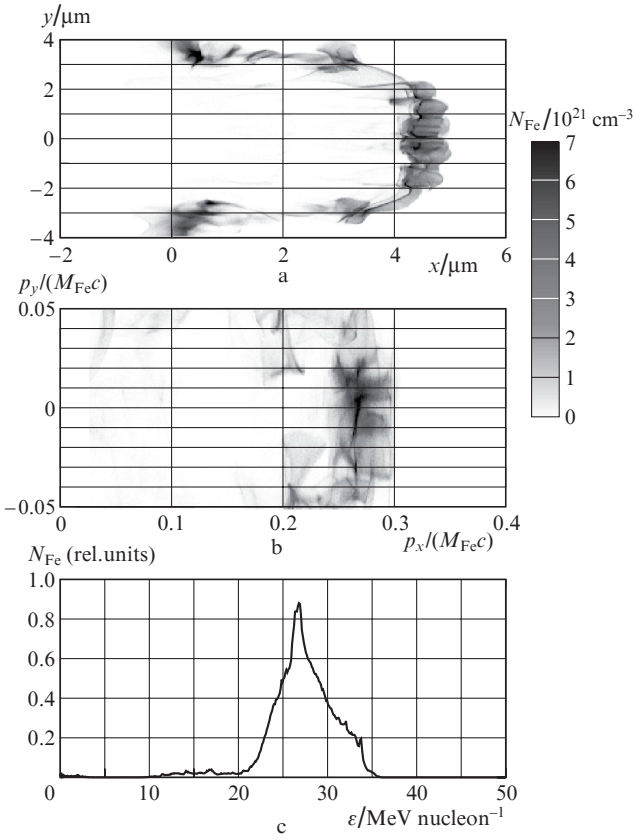

Figure 9. The same as in Fig. 8, but for a 30-fs long pulse with the use of a relativistic shutter (see text).

In conclusion we also note that the dependence of simulated data on the position of iron ion layer and the number of particles in it was hardly investigated in the present work. At the same time, the Coulomb expansion plays a major part in the beam formation. And, as shown in Ref. [43] recently, this process is strongly affected by the position of the light ion fraction. Therefore, one would expect that by varying the position of the ions under acceleration it would be possible to generate multiply charged ion beams also for relatively long pulses without using the relativistic shutter. An investigation of this question is beyond the scope of this paper.

4. Conclusions

In this paper we analysed the feasibility of generating multiply charged ion beams in the interaction of ultrahigh-power laser radiation with solid targets. It was shown that the optical field of a femtosecond pulse is capable of producing multiply charged ions (for iron ions, which were employed by way of example, the ionisation multiplicity is equal to 24), which may then be accelerated to energies of the order of tens of MeV per nucleon by the same field. Although ~8-fs long pulses are required for obtaining the best results, good results can also be obtained for 15-fs long pulses and, with the use of a relativistic shutter, for arbitrarily long pulses.

The beams are formed with a relatively high degree of energy homogeneity and localisation in space, which provides high emittance values. Furthermore, large numbers of accelerated particles permit obtaining currents higher than 1 MA and peak powers of tens of terawatts. Such beams may hold interest in nuclear physics, because they are a fundamental alternative to low-current beams of high-energy ions produced with conventional accelerators.

Acknowledgements. This work was supported in part by the programme 'Extreme Light Fields and Their Applications' of the Presidium of the Russian Academy of Sciences and by the Russian Foundation for Basic Research (Grant Nos 11-02-12293-ofi-m-2011 and 12-02-31593-mol-a). The authors also express their appreciation to the Swedish National Infrastructure for Computing for providing the possibility to perform simulations with the supercomputers of the High Performance Computing Centre North (HPC2N).

References

1. Daido H., Nishiuchi M., Pirozhkov A.S. *Rep. Prog. Phys*., **75**, 056401 (2012).
2. Korzhimanov A.V., Gonoskov A.A., Khazanov E.A., Sergeev A.M. *Usp. Fiz. Nauk*., **181**, 9 (2011) [*Phys. Usp*., **54**, 9 (2011)].
3. Bulanov S.V. et al. *Phys. Lett. A*, **299**, 240 (2002).
4. Fourkal E. et al. *Med. Phys.*, **29**, 2788 (2002).
5. Tabak M. et al. *Phys. Plasmas*, **1**, 1626 (1994).
6. Borghesi M. et al. *Plasma Phys. Controlled Fusion*, **43**, A267 (2001).
7. Cowan T. et al. *Phys. Rev. Lett*., **92**, 204801 (2004).
8. Hegelich B.M. et al. *Nature*, **439**, 441 (2006).
9. Schwoerer H. et al. *Nature*, **439**, 445 (2006).
10. Silva L.O. et al. *Phys. Rev. Lett*., **92**, 015002 (2004).
11. Yin L. et al. *Phys. Plasmas*, **14**, 056706 (2007).
12. Esirkepov T. et al. *Phys. Rev. Lett*., **92**, 175003 (2004).
13. Macchi A. et al. *Phys. Rev. Lett*., **94**, 165003 (2005).
14. Korzhimanov A.V., Gonoskov A.A., Kim A.V., Sergeev A.M. *Pis'ma Zh. Eksp. Teor. Fiz*., **86**, 662 (2007) [*JETP Lett*., **86**, 577 (2008)].
15. Gonoskov A.A. et al. *Phys. Rev. Lett*., **102**, 184801 (2009).
16. Henig A. et al. *Phys. Rev. Lett*., **103**, 245003 (2009).
17. Tahir N.A. et al. *Phys. Rev. Lett*., **95**, 035001 (2005).
18. Korzhimanov A.V. et al. *Phys. Rev. Lett*., **109**, 245008 (2012).
19. Milosevic N., Krainov V.P., Brabec T. *Phys. Rev. Lett*., **89**, 193001 (2002).
20. Hetzheim H.G., Keitel C.H. *Phys. Rev. Lett*., **102**, 083003 (2009).
21. Keldysh L.V. *Zh. Eksp. Teor. Fiz*., **47**, 1945 (1964).
22. Chin S.L., in *Advances in Multiphoton Processes and Spectroscopy* (Singapore: World Scientific, 2004) Vol. 16, p. 249.
23. Ilkov F.A., Decker J.E., Chin S.L. *J. Phys. B: At. Mol. Opt. Phys*., **25**, 405 (1992).
24. Popov V.S. *Usp. Fiz. Nauk*., **174**, 921 (2004) [*Phys. Usp*., **47**, 855 (2004)].
25. Ammosov M.V., Delone N.B., Krainov V.P. *Zh. Eksp. Teor. Fiz*., **91**, 2008 (1986).
26. Landau L.D., Lifshits E.M. *Quantum Mechanics: Nonrelativistic Theory* (Oxford: Pergamon, 1977; Moscow: Fizmatlit, 2008).
27. Nakamura T. et al. *Phys. Plasmas*, **17**, 113107 (2010).
28. Sgattoni A. et al. *Phys. Rev. E*, **85**, 036405 (2012).
29. Cattani F. et al. *Phys. Rev. E*, **62**, 1234 (2000).
30. Siminos E. et al. *Phys. Rev. E*, **86**, 056404 (2012).
31. Filbet F., Sonnendrocker E., Bertrand P. *J. Comput. Phys*., **172**, 166 (2001).
32. Yee K. *IEEE Trans. Antennas Propag*., **14**, 302 (1966).
33. Burza M. et al. *New J. Phys*., **13**, 013030 (2011).
34. Korzhimanov A.V., Gonoskov A.A. *Proc. 22nd Int. Conf. on Numerical Simulations of Plasma* (Princeton, USA, 2011).
35. http://www.ipfran.ru/english/structure/lab334/simlight.html.
36. Bulanov S.S. et al. *Phys. Rev. E*, **78**, 026412 (2008).
37. Brantov A.V. et al. *Phys. Plasmas*, **13**, 122705 (2006).
38. Brantov A.V. et al. *Phys. Plasmas*, **16**, 043107 (2009).
39. Esirkepov T. et al. *Phys. Rev. Lett*., **96**, 105001 (2006).
40. Brantov A.V. et al. *Nucl. Instrum. Methods Phys. Res., Sect. A*, **653**, 62 (2011).
41. Nam I. et al. *Phys. Rev. E*, **85**, 026405 (2012).
42. Vshivkov V.A. et al. *Phys. Plasmas*, **5**, 2727 (1998).
43. Govras E.A., Bychenkov V.Yu., Brantov A.V. *Zh. Eksp. Teor. Fiz*., **141**, 859 (2012) [*JETP*, **114**, 748 (2012)].